Appendix C

Appendix to Chapter 4: Manipulating the ABCs of Self-Assembly via Low-χ Block Polymer Design

1. Chang, A. B.; Bates, C. M.; Lee, B.; Garland, C. M.; Jones, S. C.; Spencer, R. K.; Matsen, M. W.; Grubbs, R. H. Manipulating the ABCs of Self-Assembly via Low-χ Block Polymer Design. *Proc. Natl. Acad. Sci.* **2017**, *114*, 6462–6467.

2. Sunday, D. F.;* Chang, A. B.;* Liman, C. D.; Gann, E.; DeLongchamp, D. M.; Matsen, M. W.; Grubbs, R. H.; Soles, C. L. Evidence for Backbone Flexibility of Bottlebrush Block Copolymers Driven by Low-χ Assembly. **2018**. *submitted.* (**Corresponding authors.*)

Table of Contents

C-1 Synthesis of LSO and LSL' Brush Triblock Polymers

LSO and LSL' brush triblock polymers were synthesized by the grafting-through ring-opening metathesis polymerization (ROMP) of norbornene-functionalized macromonomers (MMs) (Scheme C.1, Tables 4.1–4.2). The poly(D,L-lactide) (PLA, L) MM ($M_\mathrm{n,L\text{-}MM}$ = 4410 g/mol, $Đ$ = 1.14); polystyrene (PS, S) MM ($M_\mathrm{n,S\text{-}MM}$ = 2650 g/mol, $Đ$ = 1.03); and poly(ethylene oxide) (PEO, O) MM ($M_\mathrm{n,O\text{-}MM}$ = 2280 g/mol, $Đ$ = 1.04) were synthesized as described in Appendix A-2. The same macromonomers were used for all LSO and LSL' syntheses.

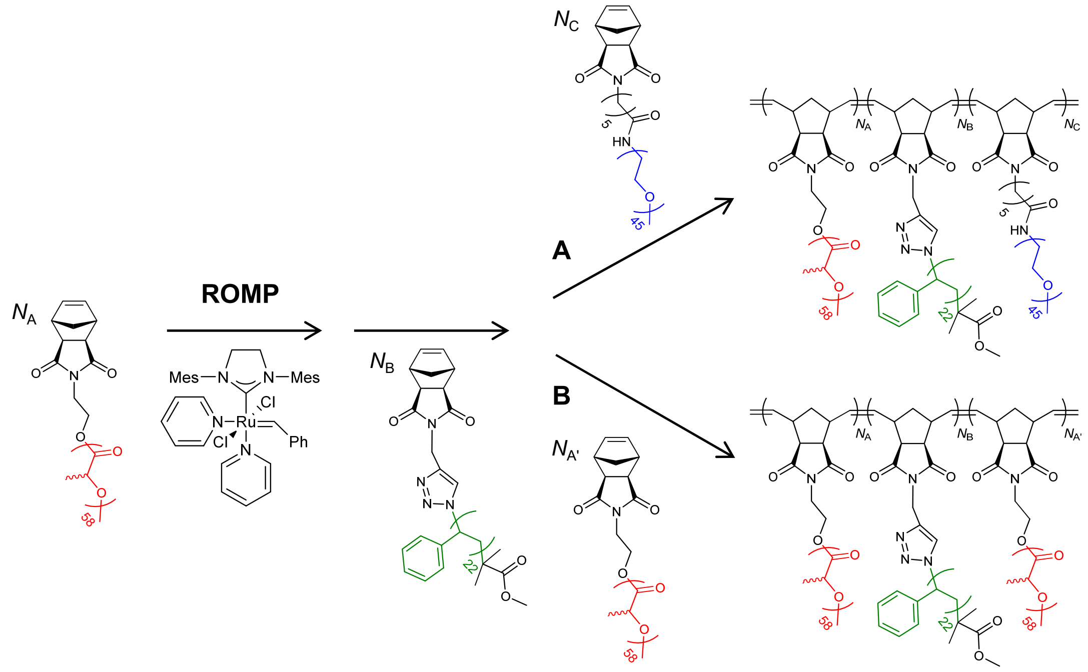

Scheme C.1: Synthesis of brush triblock polymers by ring-opening metathesis polymerization (ROMP): (*A*) LSO, (*B*) LSL'. Red, green, and blue structures represent poly(D,L-lactide) (L), polystyrene (S), and poly(ethylene oxide) (O) side chains, respectively. This color scheme is used in all figures.

In a typical triblock terpolymer synthesis, in a glovebox under inert argon atmosphere, three separate vials were prepared containing stock solutions of each MM in dry DCM. For example, for the synthesis of LSO*, vial A: PLA MM (4.15 g, 31.7 mL); vial B: PS MM (2.46 g, 18.5 mL); vial C: PEO MM (1.18 g, 10.3 mL). A fourth vial was prepared with the ruthenium catalyst (32.6 mg, 0.045 mmol) in 1.30 mL dry DCM (34.6 mM).

To a 4 mL vial equipped with a stir bar, 1.50 mL of the PLA MM stock solution was added (0.0386 mmol, 27 equiv.). The polymerization was initiated by adding 48.4 µL of the catalyst stock solution to the stirring solution (0.00167 mmol, 1.0 equiv.). After 15 minutes, a small aliquot (L, <0.1 mL) was extracted and quenched with ethyl vinyl ether in THF for subsequent analysis by SEC. After the aliquot was collected, 0.83 mL of the PS MM stock solution was added to the reaction vial (0.0416 mmol, 25 equiv.). After an additional 30 minutes, a small aliquot (LS, <0.1 mL) was extracted and quenched with ethyl vinyl ether in THF, and 0.17 mL of the PEO MM stock solution was added to the reaction vial (0.00854 mmol, 5.1 equiv.). After an additional 90 minutes, the vial was removed from the glovebox and quenched with 0.25 mL (10% reaction volume) ethyl vinyl ether. A third aliquot (LSO, <0.1 mL) was collected. After stirring for 30 minutes, the solution was added dropwise to 15 mL cold diethyl ether (−78 °C). The mixture was centrifuged at 10000 rpm for 2 minutes, then the clear supernatant was poured off. The solid was dried *in vacuo* for 24 hours to yield LSO* as an off-white powder (0.27 g, 83%).

This method also enables efficient synthesis of a variety of LSO and LSL' brush triblock terpolymers with varying backbone degrees of polymerization (N_{A}, N_{B}, N_{C} and N_{A}, N_{B}, $N_{\mathrm{A'}}$ respectively), controlled directly by the volume ratios of MM stock solutions. For the series LSO-N_{C}, in which N_{A} and N_{B} are fixed and N_{C} is varied between 0 and 20, the synthetic approach can guarantee fixed N_{A}, N_{B} for all 10 samples in the series. A large batch of the PLA-PS diblock copolymer was synthesized then split to 10 vials, and a different volume of PEO MM stock solution was added to each vial (Table 4.1, Scheme C.2). The same approach was employed to synthesize an analogous series of LSL'-$N_{\mathrm{A'}}$ brush triblock copolymers with fixed N_{A} and N_{B} and variable $N_{\mathrm{A'}}$ (Table 4.2).

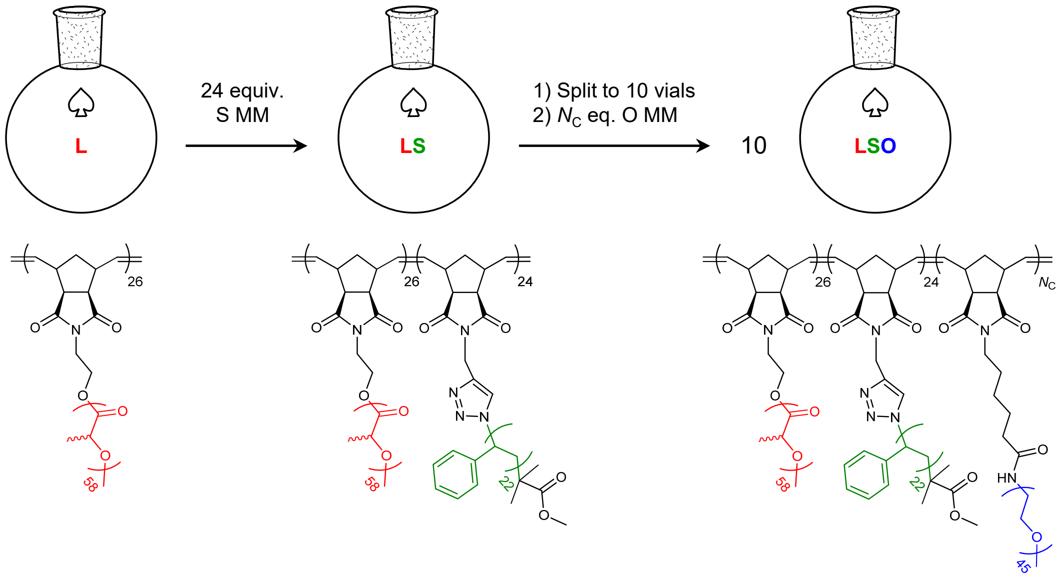

Scheme C.2: Synthesis of LSO-N_{C} brush triblock terpolymers with *guaranteed* fixed N_{A} and N_{B}. A large batch of the PLA macromonomer (L MM) is polymerized by ROMP to the L brush homopolymer. Addition of the PS macromonomer (S MM) to the same flask obtains a parent LS brush diblock copolymer with controlled N_{A} and N_{B}. The solution of LS is split to 10 vials, and an appropriate volume of a stock solution of PEO macromonomer (O MM) is added to each vial. In this way, 10 different LSO brush triblock terpolymers are obtained, each with the same N_{A} and N_{B} and variable N_{C}. LSL' brush triblock copolymers were synthesized in the same way (replacing O MM with L MM in the last step).

C-2 Molecular Characterization

C-2.1 *Instrumentation: ^{1}H NMR and SEC*

^{1}H NMR spectra were recorded on a Varian Inova 500 MHz instrument. Deuterated chloroform was used as the solvent, and chemical shifts are reported in parts per million (ppm) using residual protonated solvent as an internal standard ($CHCl_3$, ^{1}H 7.26 ppm).

Size-exclusion chromatography (SEC) data was obtained on one of two instruments depending on the composition of the sample. All polymers containing PEO (*i.e.*, the LSO brush triblock terpolymers) were characterized using tetrahydrofuran (THF) with 1 vol% trimethylamine as the mobile phase, which eliminated artificial dragging effects presumably arising from PEO/column interactions in pure THF. The instrument (A) includes an Agilent 1100 Series pump and autosampler and two MZ-Gel SD*plus* 300×8.0 mm columns with 10 μm beads. The columns were connected in series with a Wyatt three-angle miniDAWN TREOS light scattering detector, Optilab rEX differential refractive index detector, and ViscoStar viscometer. Samples were prepared as 2 mg/mL solutions of isolated, dry polymer in THF. For polymers that did not contain PEO, samples were measured on both Instrument A and a second instrument (B), which uses an Agilent 1260 Series pump and autosampler and two Agilent PLgel MIXED-B 300×7.5 mm columns with 10 μm beads. The columns were connected in series with a Wyatt 18-angle DAWN HELEOS light scattering detector and Optilab rEX differential refractive index detector. The mobile phase was pure THF, and the measured molecular weights and dispersities agree within 1%. PEO-containing polymers benefitted from a mobile phase with 1 vol% trimethylamine, but the light scattering detector for Instrument A has fewer angles (3) than Instrument B (18).

C-2.2 *Characterization of LSO and LSL' Triblock Polymers*

The LSO and LSL' brush triblock polymers were characterized by SEC and ^{1}H NMR. Figures C.1–C.3 show representative SEC traces. Aliquots of the quenched timepoints show complete consumption of the PLA macromonomer (MM), L block, and LS diblock before subsequent blocks are added. For all samples, a single narrow peak is present for all timepoints. The absolute molecular weights of the brush triblock polymers can be determined by a combination of SEC and NMR.

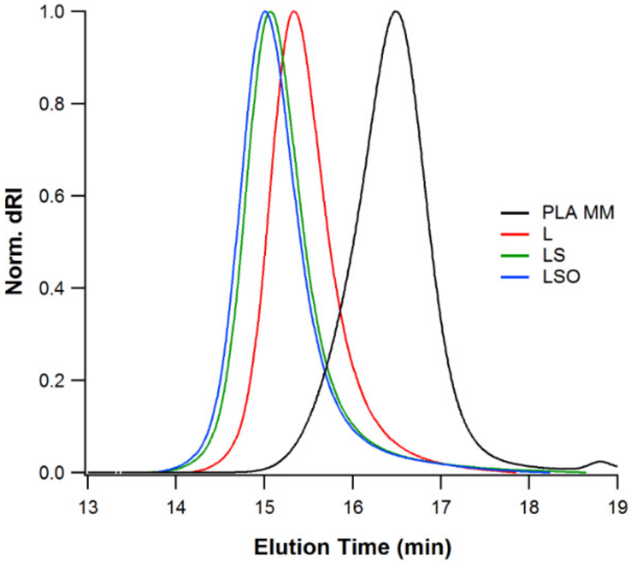

Figure C.1: Size-exclusion chromatogram (SEC) of LSO* (N_A = 28, N_B = 27, N_C = 5). The peaks are unimodal and narrow, indicating low molar mass dispersity. Complete consumption is observed at each stage prior to addition of subsequent blocks.

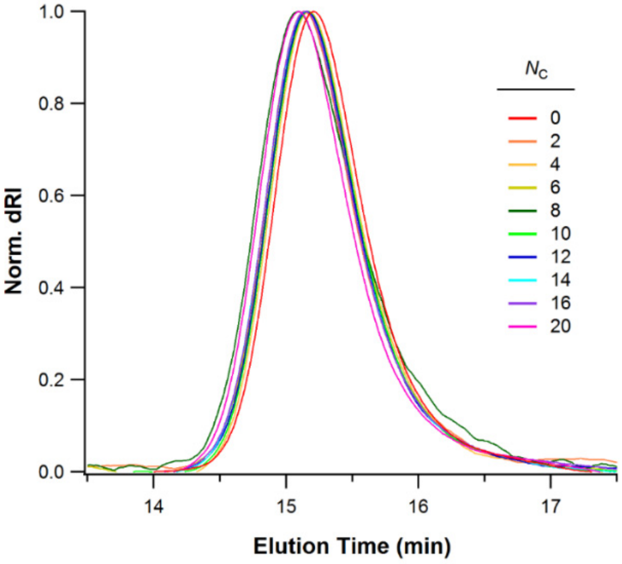

Figure C.2: SEC traces of 10 LSO-N_C triblock terpolymers with fixed N_A and N_B and variable N_C. For these triblocks, N_A = 26, N_B = 24, and $0 \leq N_C \leq 20$ (Table 4.1).

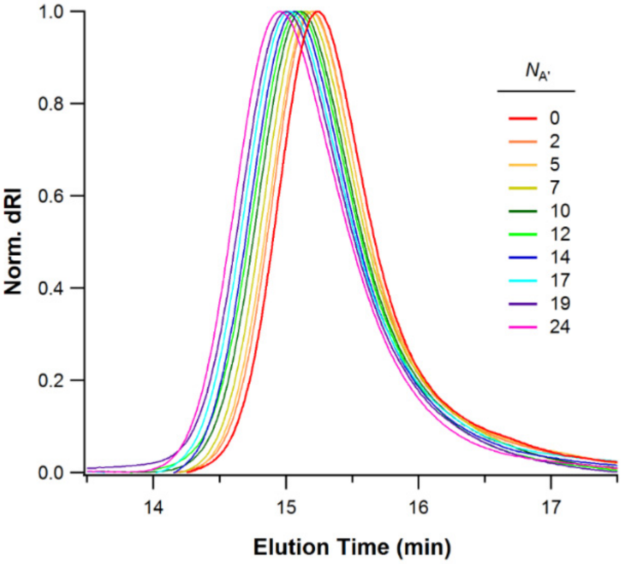

Figure C.3: SEC traces of 10 LSL'-$N_{A'}$ triblock copolymers with fixed N_A and N_B and variable $N_{A'}$. For these triblocks, $N_A = 30$, $N_B = 28$, and $0 \leq N_{A'} \leq 24$ (Table 4.2).

The following discussion describes the characterization of LSO; characterization of the simpler LSL' systems was performed in the same way. For each triblock, the aliquot of the A block (PLA) collected during synthesis was analyzed by SEC. The dn/dc value used for the PLA brush homopolymer was 0.050 mL/g, determined by assuming 100% mass elution from the columns. This value is consistent with literature reports [1]. SEC enables determination of the absolute weight-average molecular weight of the first block ($M_{w,A}$). Dividing by the dispersity ($Đ < 1.05$ for all samples) obtains the number-average molecular weight of the first block ($M_{n,A}$). In turn, dividing $M_{n,A}$ by the number-average molecular weight of the PLA MM ($M_n = 4410$ g/mol) obtains the number-average backbone degree of polymerization of the first block (N_A).

The isolated LSO triblock terpolymer was analyzed by SEC and ^{1}H NMR ($CDCl_3$, 500 MHz). For NMR, characteristic peaks for PLA, PS, and PEO were identified: L: 5.30−5.05, S: 7.22−6.32, and O: 3.77−3.60 ppm. Peak integrations (I_L, I_S, I_O) were used to calculate the relative molar fractions of each side chain (X_L, X_S, X_O) (Eqs. C-1−C-3):

$$X_L = \frac{I_L}{1 \times N_{\text{L-MM}}} \qquad \text{Eq. C-1}$$

$$X_{\mathrm{S}} = \frac{I_{\mathrm{S}}}{5 \times N_{\mathrm{S\text{-}MM}}} \quad \text{Eq. C-2}$$

$$X_{\mathrm{O}} = \frac{I_{\mathrm{O}}}{4 \times N_{\mathrm{O\text{-}MM}}} \quad \text{Eq. C-3}$$

where $N_{\mathrm{i\text{-}MM}}$ is the degree of polymerization of the side chain (i.e., number of monomers per side chain) and the constant in the denominator is the number of integrated protons per monomer. The ratios $X_{\mathrm{S}}/X_{\mathrm{L}}$ and $X_{\mathrm{O}}/X_{\mathrm{L}}$ represent the relative backbone degrees of polymerization for the PS- and PEO-containing blocks, respectively. Because absolute N_{A} is obtained from the absolute M_{w} of the first block by SEC, the remaining backbone degrees of polymerization N_{B} and N_{C} can be determined using these ratios (Eq. C-4):

$$N_{\mathrm{i}} = \frac{X_{\mathrm{i}}}{X_{\mathrm{L}}} \times N_{\mathrm{A}} \quad \text{Eq. C-4}$$

From the backbone degrees of polymerization, the total molecular weight of each LSO brush triblock terpolymer can be calculated (M_{n}, Eq. C-5):

$$M_{\mathrm{n}} = N_{\mathrm{A}} M_{\mathrm{n,L\text{-}MM}} + N_{\mathrm{B}} M_{\mathrm{n,S\text{-}MM}} + N_{\mathrm{C}} M_{\mathrm{n,O\text{-}MM}} \quad \text{Eq. C-5}$$

C-3 Self-Consistent Field Theory (SCFT): Methods

Following the overview of SCFT in Section 4-3, further details and discussion of chain parameters are provided here. For each side chain (PLA, PS, and PEO), data for the statistical segment lengths (a), densities (ρ), monomer molar mass (m_{m}), and number of monomers per reference volume ($V_{\mathrm{ref}} = 118$ Å^3) (n_{v}) are included in Table C.1. Values for PLA,[2] PS,[3] and PEO[3] were obtained from literature reports.

Based on previous work in the literature,[4] the side chains are not expected to extend significantly more than the unperturbed end-to-end distance, $R_0 = aN^{1/2}$ (where a is the statistical segment length and N is the total backbone degree of polymerization) (Figure 4.2). The stretching of cylindrical brushes (*i.e.*, bottlebrush polymers) is far less than the stretching of planar brushes, which itself is typically less than 50% of the unperturbed length.[5] Previous SCFT treatment of bottlebrush polymers has assumed that the side chains stretch approximately 10% more than the unperturbed chain lengths and that the extent of stretching is uniform throughout the brush (*i.e.*, similar at the chain ends and the middle of the brush).[4] In this report, we did not increase the segments of the sidechains as was done previously to account for end effects that become important for small N.

For the backbone, we employ a worm-like chain of fixed contour length (L) with a certain persistence length (ξ_b). The side chains are attached to the backbone with a uniform spacing of $\Delta L = 6.2$ Å equal to the length of one polynorbornene backbone unit, such that the total length of the backbone is $L = N\Delta L$. For LSO*, the contour length is estimated as follows: $L = (N_A + N_B + N_C) \times 0.62$ nm $= (28 + 27 + 5) \times 0.62$ nm $=$ **37 nm**. We set the persistence length to $\xi_b = 5\Delta L$, the same value that successfully modeled the polynorbornene backbone previously.[4] Due to the extreme side chain crowding, we assume that the backbone only experiences interactions with its grafted side chains, which implies that its interaction energy remains constant and thus can be omitted from the Hamiltonian. By also ignoring the volume of the backbone, there is no field whatsoever acting on the backbone, which simplifies the calculation. The remaining fields [$w_L(\mathbf{r})$, $w_S(\mathbf{r})$ and $w_O(\mathbf{r})$], acting on the three different side chain species, were solved for the usual self-consistent conditions of an incompressible melt.

Table C.1: SCFT input parameters for the grafted PLA, PS, and PEO side chains: a is the statistical segment length, ρ is the bulk density, m_m is the monomer molar mass, and n_V is the number of monomers per reference volume ($V_{ref} = 118$ Å^3). All data were obtained from literature sources[2-3] and reported at 140 °C, the annealing temperature.

	PLA	**PS**	**PEO**
Structure	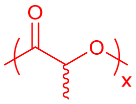	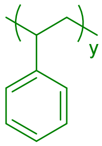	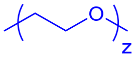
a (Å)	6.4	6.7	6.0
ρ (g cm^{-3})	1.152	0.969	1.064
m_m (g mol^{-1})	72.10	104.15	44.05
n_V	1.135	0.661	1.716

C-4 Transmission Electron Microscopy (TEM)

Transmission electron microscopy (TEM) was performed on an FEI Tecnai F30 instrument operated at 300 keV. A 10 µm objective aperture was used in order to enhance contrast. LSO* was annealed by channel-die alignment at 140 °C. A bulb extruded from the end of the die was trimmed using a double-edged razor blade to expose a face with superficial area under 200 µm × 200 µm. The sample was stained over ruthenium tetroxide (RuO_4) vapors for 4 hr. RuO_4 vapors were generated in situ by mixing 50 mg ruthenium (III) chloride hydrate and 3.0 mL sodium hypochlorite solution in a 20 mL vial. After staining, the samples were microtomed at room temperature and cut speed 1.0 mm/s using a Leica EM UC7 ultramicrotome and Diatome diamond knife. Thin sections (~70 nm thick) were floated off water onto holey carbon-coated copper grids (SPI, 200 mesh). TEM images for LSO* are shown in Figures 4.3A and C.4.

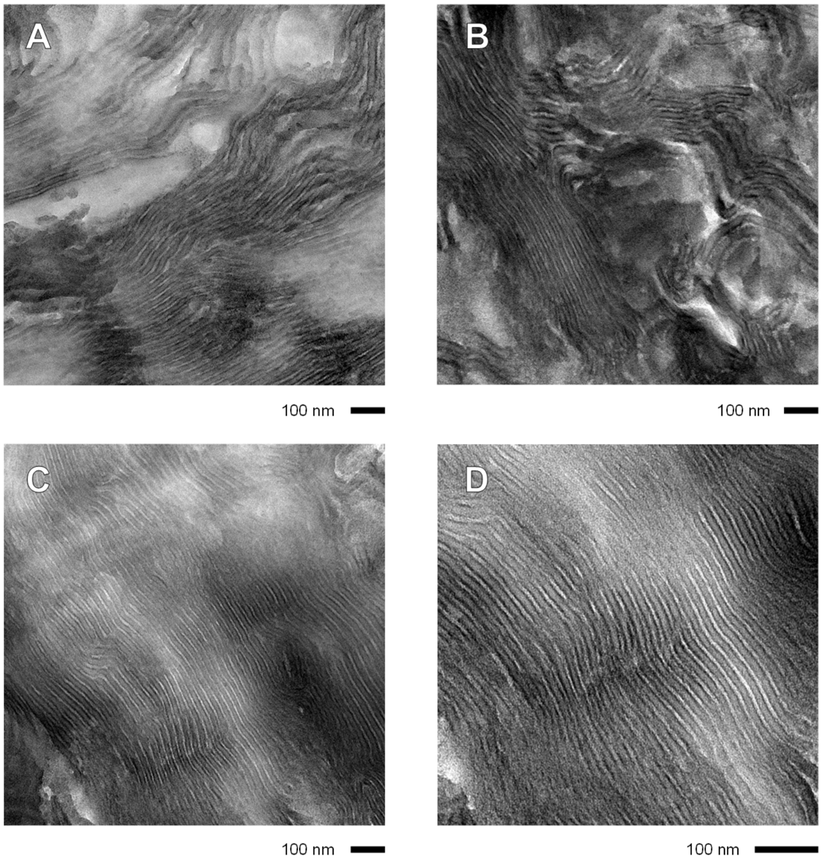

Figure C.4: (*A–C*) TEM images of different sections of LSO*. (*D*) Higher-magnification image of one area in (*C*). All images show a three-color, four-layer lamellar morphology with the same relative domain thicknesses and contrast. Compare Figure 4.3A.

TEM images for LSO-4, -10, and -14 are shown in Figure C.8. The same method was attempted to obtain images of these LSO-N_C samples. However, the channel-die aligned samples were not well-ordered, and sectioning out-of-plane resulted in non-uniform sections. Instead, sections of LSO-N_C were prepared using exactly the same films characterized by SAXS. One piece of Kapton was peeled away from the Kapton-sandwiched sample. The remaining piece, on which the polymer film remained, was stained over RuO_4 vapors for 4 hours. A small amount of EpoKwick epoxy (~10 mL) was prepared in a vial by mixing resin and hardener in a 5:1 ratio by weight. The stained film on Kapton was placed face up in a small plastic weigh boat, and ~1 mL epoxy was poured on top. After curing at room temperature overnight, the Kapton was peeled away, leaving the polymer film embedded on epoxy. The epoxy was trimmed and then embedded in a mold with additional EpoKwick epoxy. After curing at room temperature, the blocks were trimmed using a double-edged razor blade to expose a face with superficial area under 200 μm × 200 μm. The blocks were stained over RuO_4 for 24 hours to harden the material and improve contrast. After staining, the samples were microtomed at room temperature and cut speed 1.0 mm/s using a Leica EM UC7 ultramicrotome and Diatome diamond knife. Thin sections (~70 nm thick) were floated off water onto holey carbon-coated copper grids.

In our hands, it was challenging to consistently generate three-color contrast for all samples. We note that LSO* was annealed and sectioned at the University of Minnesota, whereas the LSO-N_C samples were annealed and sectioned at Caltech, contributing to the challenges associated with reproducing TEM conditions. Samples were prepared in multiple different ways for TEM, spanning variations in annealing methods (channel-die alignment, annealing between glass, annealing between Kapton), microtomy conditions (temperature, section thickness), and staining times (1 minute to 24 hours). Despite these attempts, the three-phase contrast could not be obtained for LSO-N_C samples. Based on images for LSO* and extensive other evidence (including SAXS, DSC, and SCFT) however, we believe that the LSO-N_C samples do in fact form the LAM_P morphology. The TEM images confirm that the structure is well-ordered and lamellar, but the sectioning and staining procedures may not be fully optimized to visualize the expected relative contrast.

C-5 Small-Angle X-ray Scattering (SAXS)

Small-angle X-ray scattering (SAXS) was performed at Beamline 12-ID-B at the Advanced Photon Source (APS) at Argonne National Laboratory. The samples were studied using 14 keV (0.89 Å) X-rays and a sample-to-detector distance of 2.00 m, calibrated using a silver behenate standard. SAXS data for each sample was collected parallel to the plane of the substrate (approximately 2 mm thick in the beam direction). The sample was tilted $\phi = 3°$ relative to the normal toward the detector in order to improve the signal since the lamellar samples were highly oriented perpendicular to the beam. Exposure times between 0.1 and 1 s were used for all measurements.

All LSO and LSL' brush triblock polymers were prepared for analysis by SAXS as follows: (1) Neat LSO or LSL' triblock powder (approx. 10 mg) was placed between two sheets of 25 µm thick Kapton film. (2) The sample between Kapton was placed between two glass slides. (3) The glass slides were clamped with medium binder clips (Office Depot). (4) The samples were annealed under vacuum at 140 °C for 12 hr. (5) After 12 hr, the samples were allowed to slowly cool to 25 °C under vacuum. (6) Scissors were used to cut a thin strip of the Kapton-sandwiched sample (approx. 10 × 2 × 0.07 mm, length × width × height). (7) SAXS measurements were performed normal to the sample cross-section, through the width of the sample (2 mm).

Applying modest pressure while thermally annealing brush LSO and LSL' orients the self-assembled lamellae, as evident from raw 2D SAXS patterns. For some samples, applied pressure also appears to improve the extent of order. Each dropcast sample was prepared by applying 0.3 mL of a 10 mg/mL solution of polymer in DCM onto a piece of Kapton. The solvent was allowed to evaporate in air at room temperature for 12 hours, and the film was subsequently dried under high vacuum (<50 mTorr) for 24 hours to remove any residual solvent.

C-6 Supporting Data for LSO-N_C Series

Table C.2: Glass transition temperatures (T_g), LAM spacings (d^*, d LAM$_{//}$), and assigned morphologies for LSO-N_C (fixed N_A and N_B and variable N_C). See Table 4.1 for full molecular characterization data and Figures C.6–C.7 for full SAXS analysis.

Sample	f_O [a]	T_g (°C) [b]	d^* LAM$_\perp$ (nm) [c]	d LAM$_{//}$ (nm) [d]	Morphology
LSO-0	0.00	55.2	29.0	32.2	LAM$_2$
LSO-2	0.02	53.1	27.9	30.1	LAM$_P$
LSO-4	0.05	50.1	27.0	29.8	LAM$_P$
LSO-6	0.07	47.1	26.8	27.6	LAM$_P$
LSO-8	0.09	42.1	26.5	27.0	LAM$_P$
LSO-10	0.11	35.3	25.8	26.2	LAM$_P$
LSO-12	0.13	30.4	25.2	26.1	LAM$_P$
LSO-14	0.15	30.2	24.6	25.9	LAM$_P$
LSO-16	0.17	29.1	24.5	25.0	LAM$_P$
LSO-20	0.20	21.2	23.6	24.2	LAM$_P$

[a] Volume fraction of the C block (O, PEO).

[b] Determined from DSC derivative curves of the second heating cycle. Only one T_g is observed for each sample.

[c] Lamellar period, $d^* = 2\pi/q^*$, determined by SAXS and reported at 25 °C. Note: d^* is the period of lamellae stacked normal to the beam, identical to $a_\perp$ indexed to the $P1$ space group.

[d] Spacing of lamellae in-plane, Note: d LAM$_{//} = a_{//}$ indexed to $P1$.

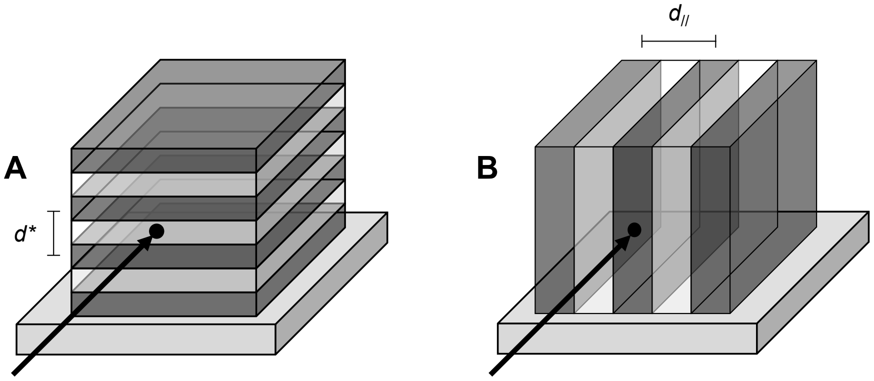

Figure C.5: Structures and relevant domain spacings indexed by SAXS. Black and white layers represent two different domains; for simplicity in visualizing the parameters, only two domains are illustrated for lamellae (whereas LAM$_3$ and LAM$_P$ each have three domains). The substrate is shown at the bottom of each sample, and the arrow indicates the direction of the X-ray beam. (*A*) LAM stacked normal to the beam. The relevant spacing is d^*, the lamellar period discussed in this report. (*B*) LAM stacked in-plane with the beam. The relevant spacing is $d_{//}$.

Figure C.6 (Part 1/3)

Raw 2D SAXS data for LSO-N_C indexed (*left*) to the $P1$ space group along the perpendicular direction, corresponding to lamellae stacked normal to the beam (LAM$_\perp$) and (*right*) to the $P1$ space group along the parallel direction, corresponding to lamellae stacked in-plane with the beam (LAM$_{//}$). The relevant parameters, provided in nanometers, are the lamellar periods $d^* = d$ LAM$_\perp$ and $d_{//} = d$ LAM$_{//}$. Green dots superimposed on the images indicate the expected peak positions. See Table C.2 for an overview of the indexed data.

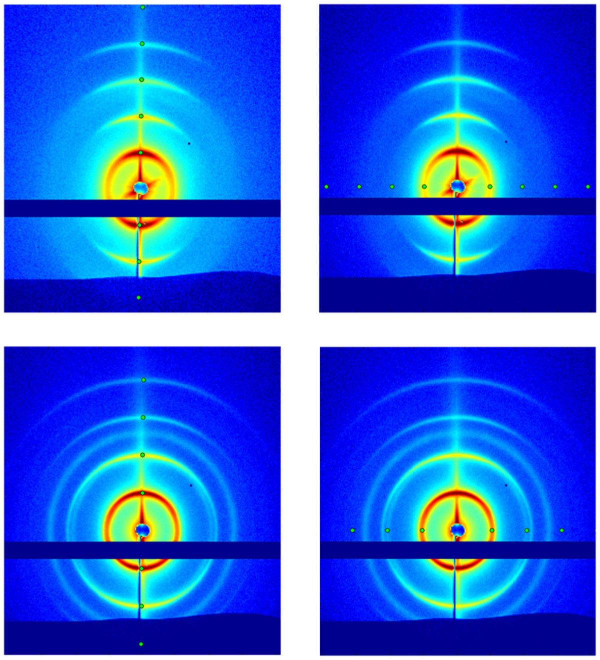

LSO-0
d^* = 29.0
d LAM$_{//}$ = 32.2

LSO-2
d^* = 27.9
d LAM$_{//}$ = 30.1

Figure C.6 (Part 2/3)

Raw 2D SAXS data for LSO-N_C indexed (*left*) to the *P*1 space group along the perpendicular direction, corresponding to lamellae stacked normal to the beam (LAM⊥) and (*right*) to the *P*1 space group along the parallel direction.

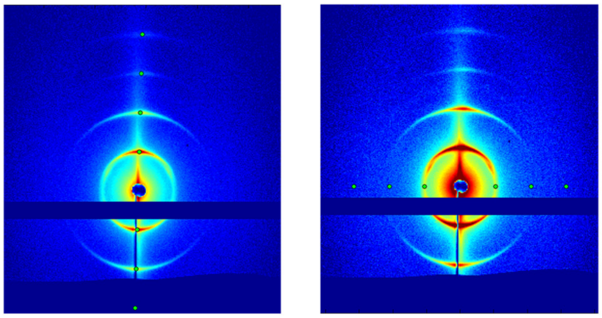

LSO-4
d^* = 27.0
d LAM$_{//}$ = 29.8

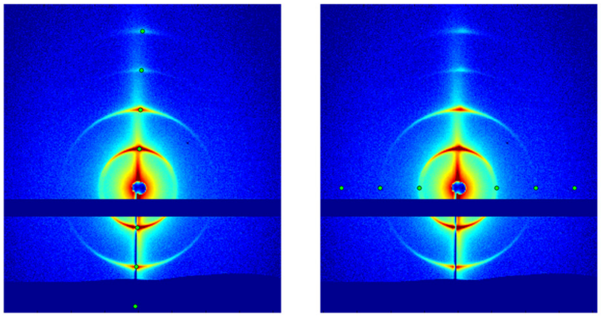

LSO-6
d^* = 26.8
d LAM$_{//}$ = 27.6

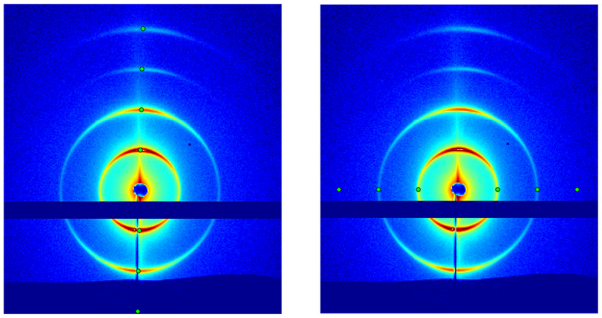

LSO-8
d^* = 26.5
d LAM$_{//}$ = 27.0

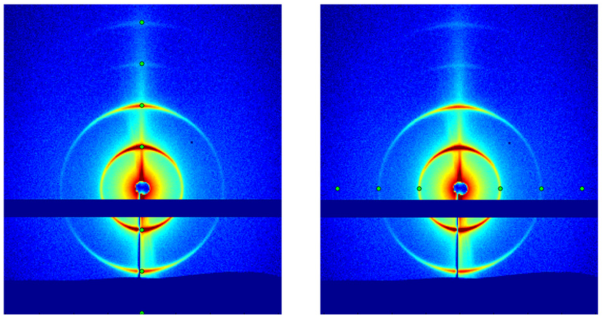

LSO-10
d^* = 25.8
d LAM$_{//}$ = 26.2

Figure C.6 (Part 3/3)

Raw 2D SAXS data for LSO-N_C indexed (*left*) to the $P1$ space group along the perpendicular direction, corresponding to lamellae stacked normal to the beam (LAM$_\perp$) and (*right*) to the $P1$ space group along the parallel direction.

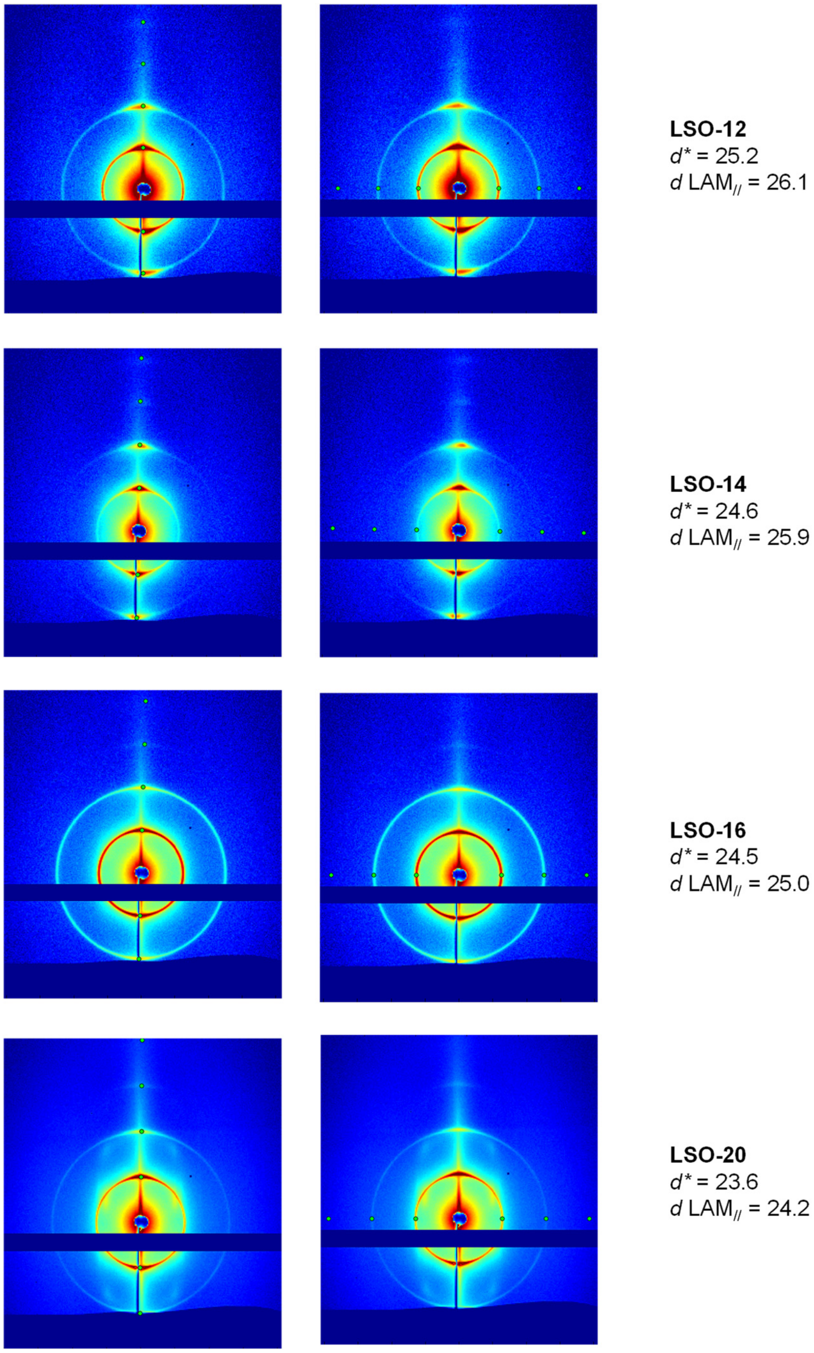

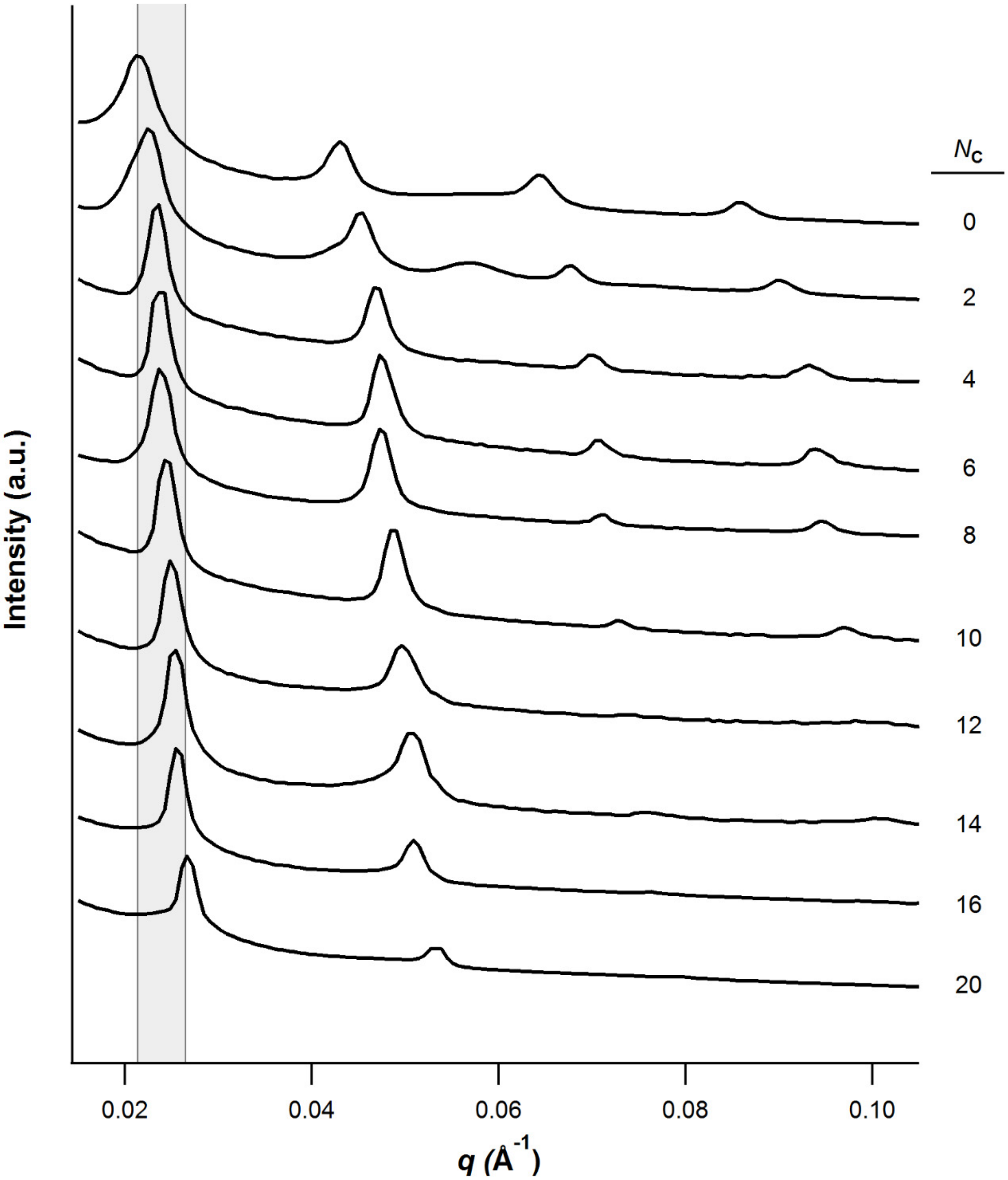

Figure C.7: Azimuthally integrated 1D SAXS patterns for LSO-N_C (fixed N_A, N_B and variable N_C), which obey $d^* \sim M^{-0.87}$. The large change in the position of q^* (and therefore $d^* = 2\pi/q^*$) across the series is emphasized by the gray box. All traces correspond to samples that self-assemble to majority LAM. Compare Fig. C.10 (LSL').

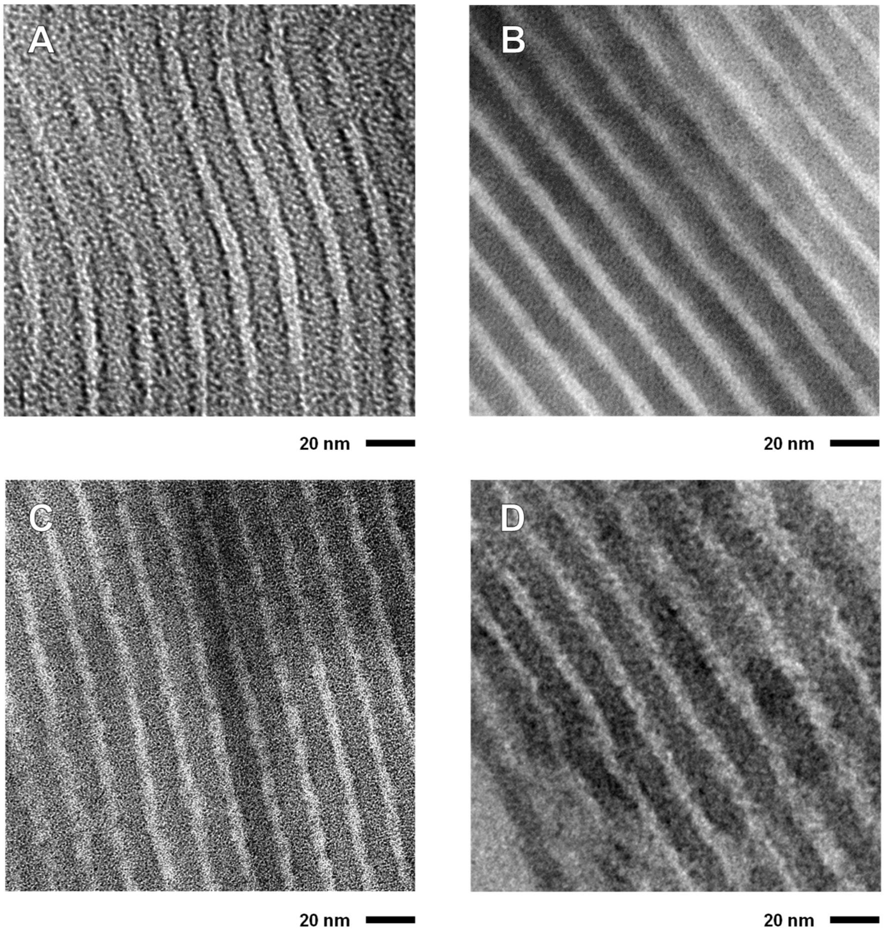

Figure C.8: TEM images of (*A*) LSO*, (*B*) LSO-4, (*C*) LSO-10, and (*D*) LSO-14. All self-assemble to lamellar morphologies, consistent with SAXS. For LSO-N_C, the domain spacings were calculated by averaging over 20 periods, and the same trend is observed by TEM and SAXS. As N_C increases, *d** decreases: *d**(LSO-4) = 19.1 nm, *d**(LSO-10) = 17.8 nm, *d**(LSO-14) = 17.7 nm. The magnitudes of the periods are smaller than those obtained from SAXS, likely due to compression of the sample upon sectioning. The three-phase contrast is clear for LSO* but is challenging to obtain for all images.

C-7 Supporting Data for LSL'-$N_{A'}$ Series

Table C.3: Glass transition temperatures (T_g), LAM spacings (d^*, d LAM$_{//}$), and assigned morphologies for LSL'-$N_{A'}$ (fixed N_A and N_B and variable $N_{A'}$). See Table 4.2 for full molecular characterization data and Figures C.9–C.10 for full SAXS analysis.

Sample	$f_{L'}$[a]	T_g (°C)[b]	d^* LAM$_{\perp}$ (nm)[c]	d LAM$_{//}$ (nm)[d]	Morphology
LSL'-0	0.00	57.1	32.9	39.2	LAM$_2$
LSL'-2	0.05	56.3	31.3	36.0	LAM$_2$
LSL'-5	0.09	55.6	29.6	35.8	LAM$_2$
LSL'-7	0.13	56.3	28.6	27.8	LAM$_2$
LSL'-10	0.16	56.1	27.8	28.2	LAM$_2$
LSL'-12	0.20	55.9	27.4	27.9	LAM$_2$
LSL'-14	0.23	56.9	26.7	29.9	LAM$_2$
LSL'-17	0.26	56.2	26.6	28.8	LAM$_2$
LSL'-19	0.28	55.9	26.2	28.5	LAM$_2$
LSL'-24	0.33	56.3	25.7	27.6	LAM$_2$

[a] Volume fraction of the variable-length PLA block (L').

[b] Determined from DSC derivative curves of the second heating cycle.

[c] Lamellar period, $d^* = 2\pi/q^*$, determined by SAXS and reported at 25 °C. Note: d^* is the period of lamellae stacked normal to the beam, identical to $a_{\perp}$ indexed to the $P1$ space group.

[d] Spacing of lamellae in-plane, Note: d LAM$_{//} = a_{//}$ indexed to $P1$.

Figure C.9 (Part 1/3)

Raw 2D SAXS data for LSL'-$N_{A'}$ indexed (*left*) to the *P*1 space group along the perpendicular direction, corresponding to lamellae stacked normal to the beam (LAM$_{\perp}$) and (*right*) to the *P*1 space group along the parallel direction, corresponding to lamellae stacked in-plane with the beam (LAM$_{//}$). The relevant parameters, provided in nanometers, are the lamellar periods $d^* = d$ LAM$_{\perp}$ and $d_{//} = d$ LAM$_{//}$. Green dots superimposed on the images indicate the expected peak positions. See Table C.3 for an overview of the indexed data.

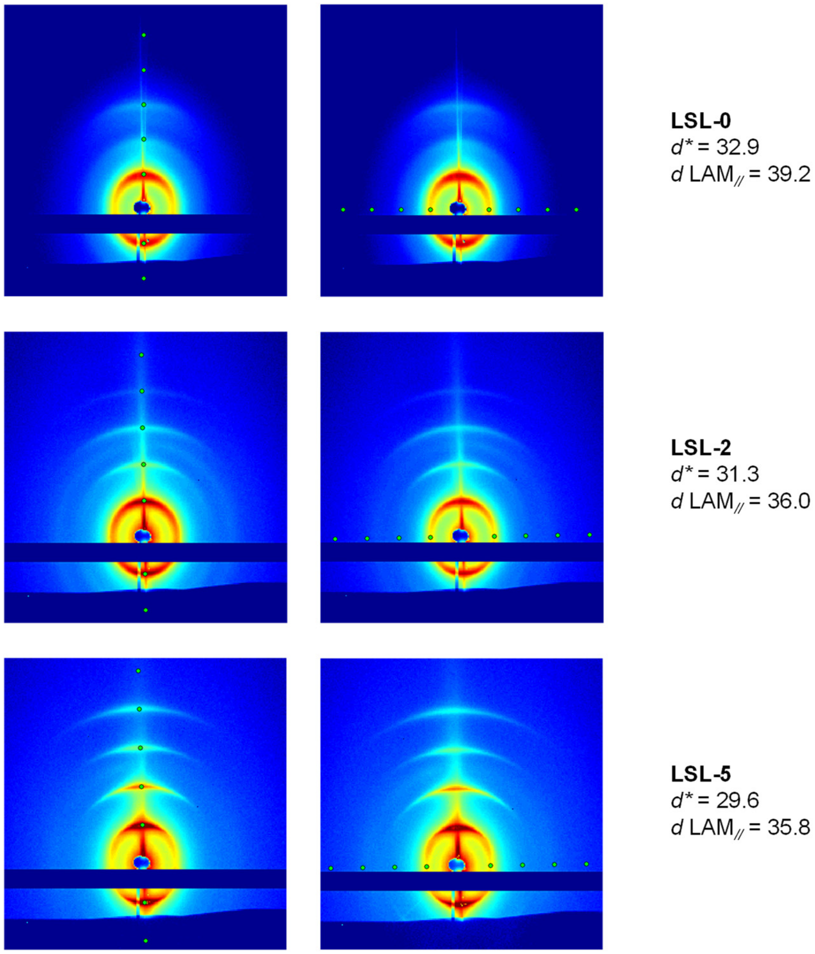

Figure C.9 (Part 2/3)

Raw 2D SAXS data for LSL'-$N_{A'}$ indexed (*left*) to the *P*1 space group along the perpendicular direction, corresponding to lamellae stacked normal to the beam (LAM⊥) and (*right*) to the *P*1 space group along the parallel direction.

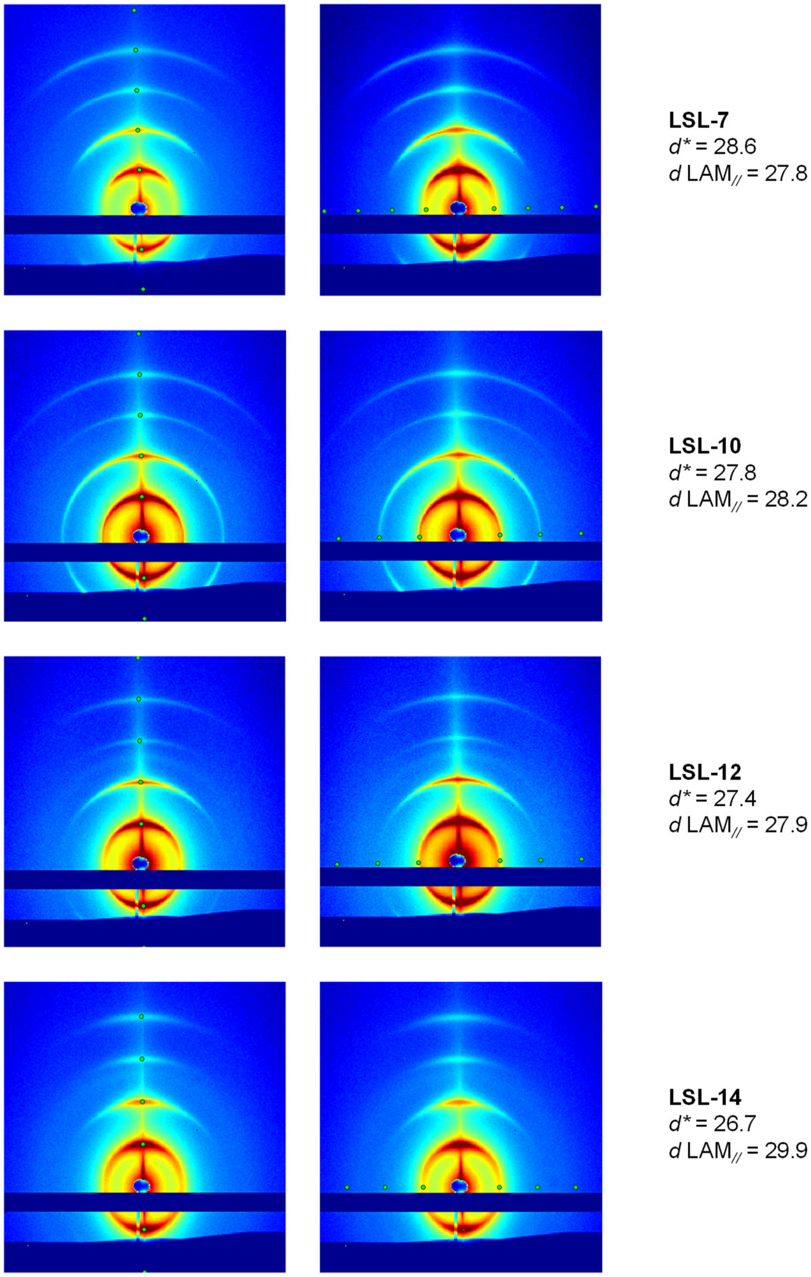

Figure C.9 (Part 3/3)

Raw 2D SAXS data for LSL'-$N_{A'}$ indexed (*left*) to the $P1$ space group along the perpendicular direction, corresponding to lamellae stacked normal to the beam ($\mathrm{LAM}_{\perp}$) and (*right*) to the $P1$ space group along the parallel direction.

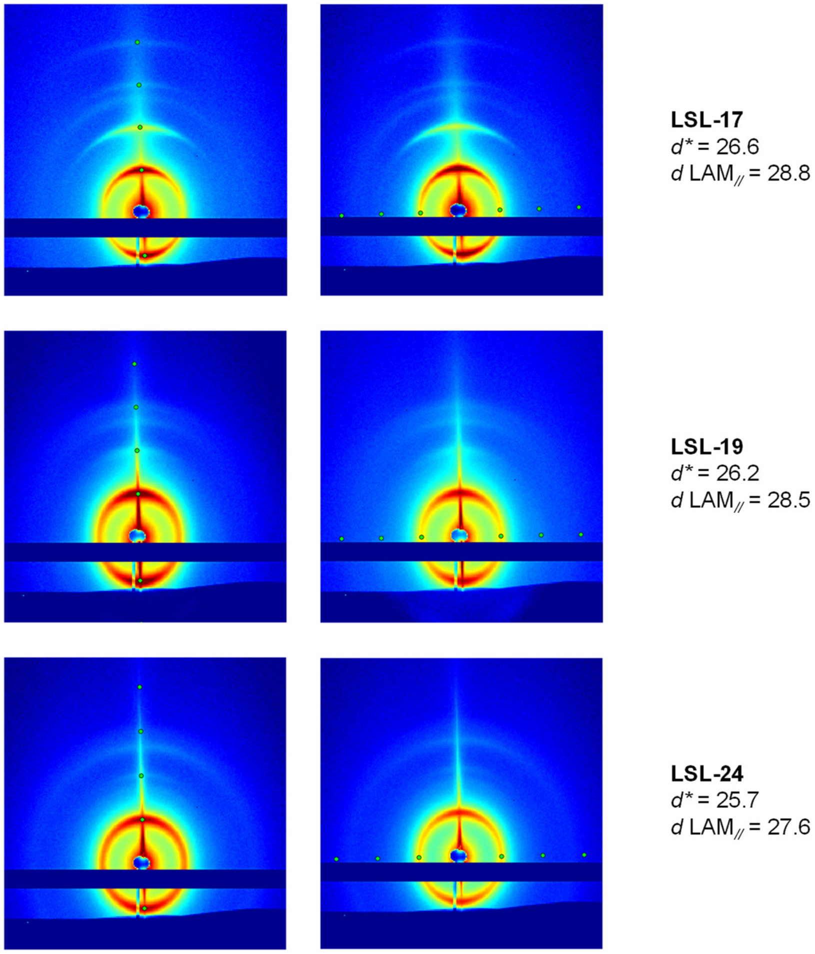

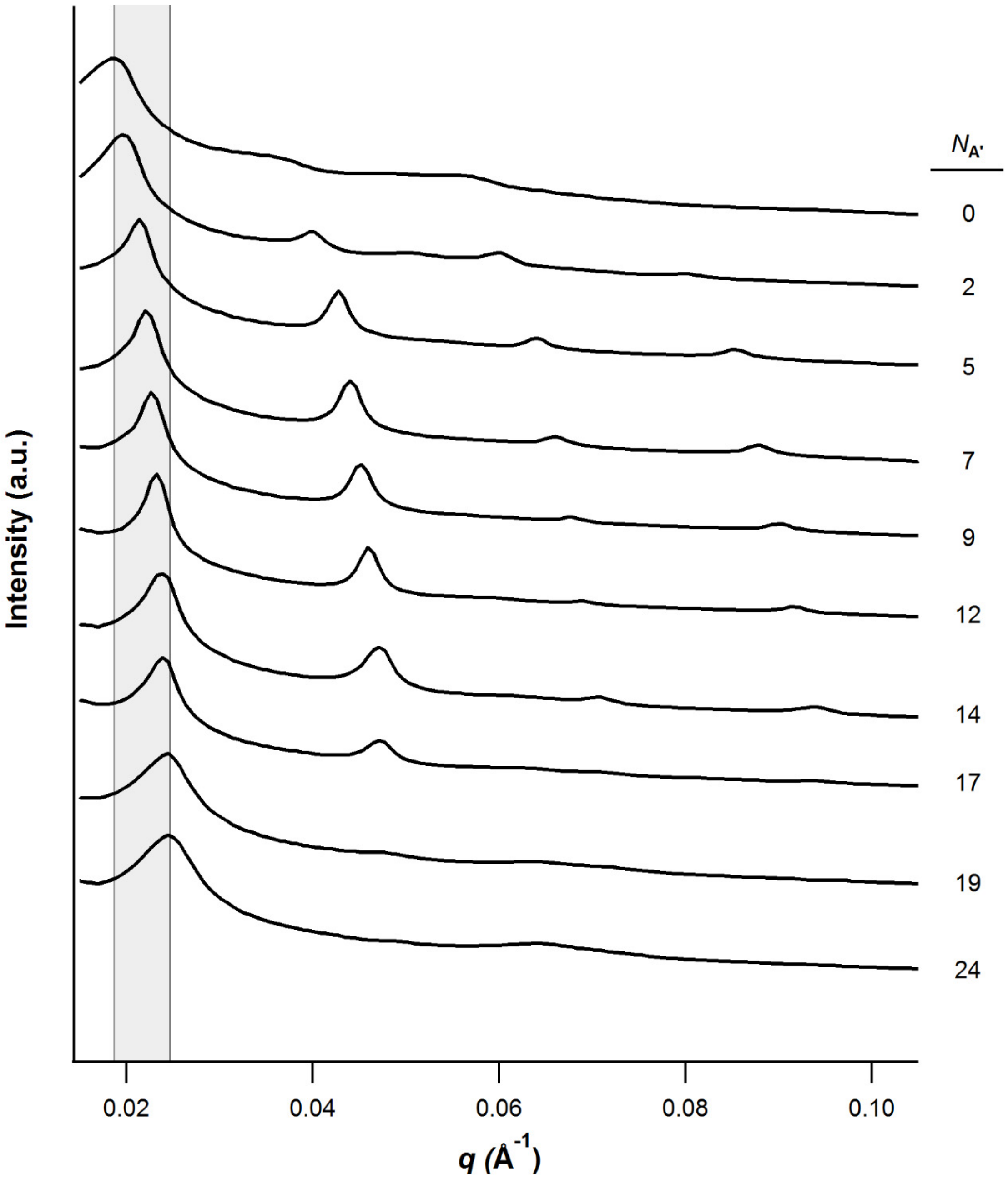

Figure C.10: Azimuthally integrated 1D SAXS patterns for LSL' brush triblock copolymers with fixed N_A and N_B and variable $N_{A'}$. The LSL' series was synthesized from a common parent LS diblock in the same way as LSO with variable N_C. The large change in the position of q^* (and therefore $d^* = 2\pi/q^*$) across the series is emphasized by the gray box. All traces correspond to samples that self-assemble to majority LAM (*i.e.,* LAM$_2$). Compare Figure C.7 (LSO).

C-8 Differential Scanning Calorimetry (DSC)

DSC data was collected on a TA Instruments Q2000 under dry nitrogen atmosphere. The samples were heated and cooled between −85 and 120 °C at 20 °C, 10 °C, and 5 °C/min. The reported values of the glass transition temperatures (T_g) were determined from derivative curves of the second heating cycle (20 °C/min). For each sample, about 10 mg of polymer was hermetically sealed in a Tzero aluminum pan.

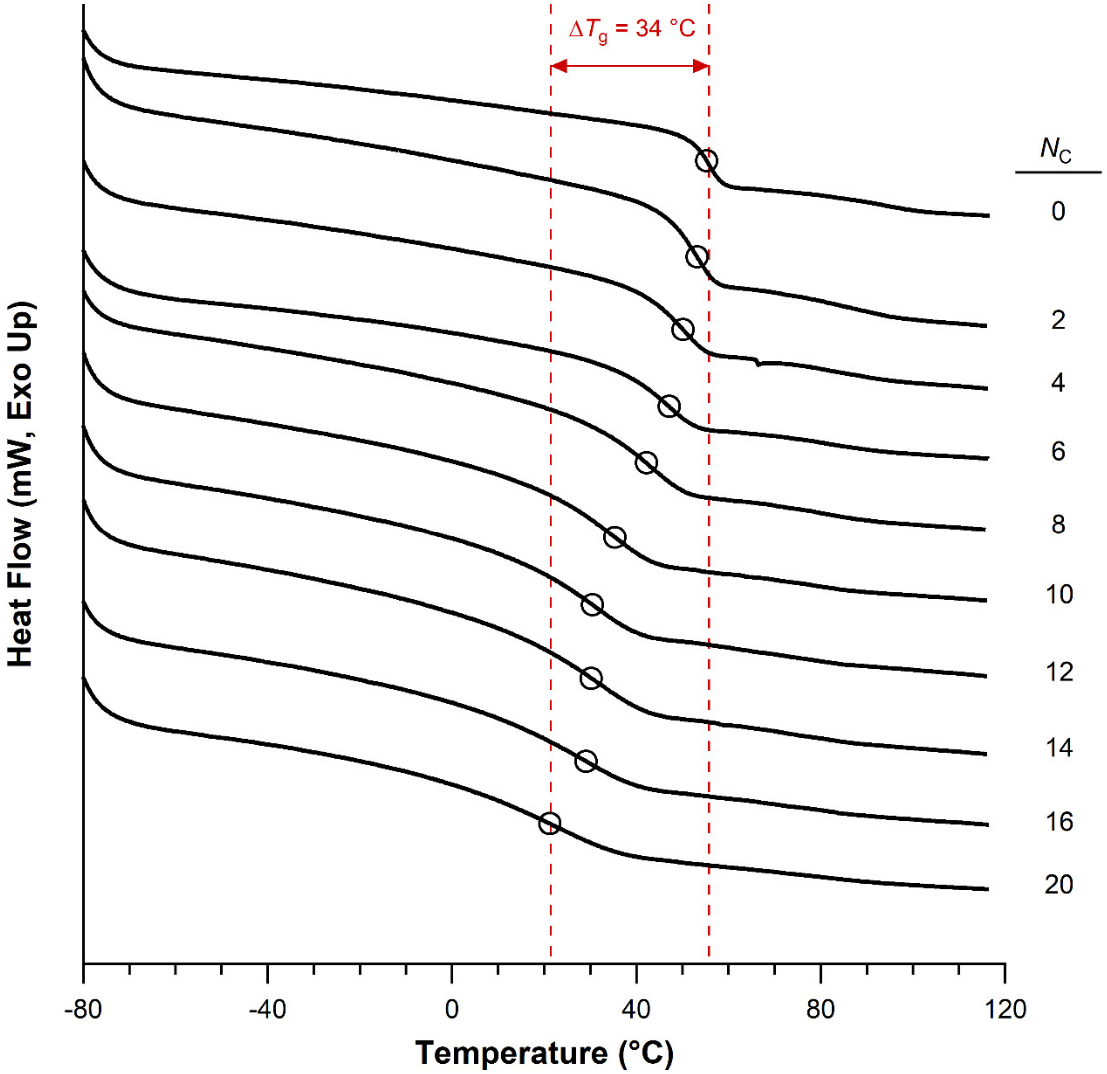

Figure C.11: DSC data for 10 LSO-N_C triblock terpolymers ($0 \le N_C \le 20$). Traces correspond to data collected upon heating from −85 °C to 120 °C at 20 °C/min. We note that under these conditions, the glass transitions of pure PLA, PS, and PEO are not observed. Open circles (○) indicate the positions of T_g, determined from the corresponding derivative curves. As N_C (and therefore the PEO content) increases, T_g decreases. Compare Fig. C.12 (LSL').

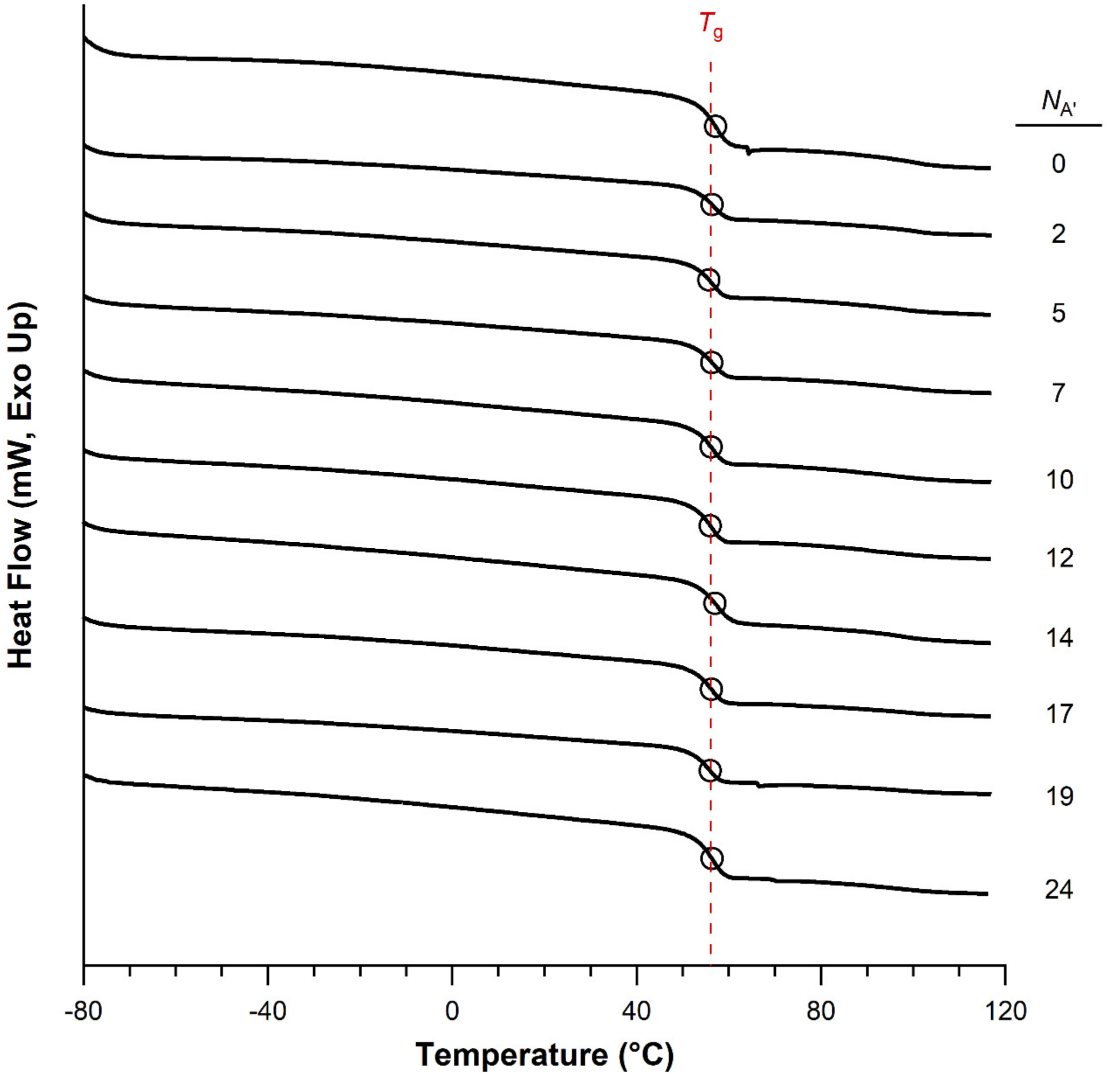

Figure C.12: DSC data for 10 LSL'-$N_{A'}$ triblock terpolymers ($0 \leq N_{A'} \leq 24$). Traces correspond to data collected upon heating from −85 °C to 120 °C at 20 °C/min. We note that under these conditions, the glass transition of PS is not observed. Open circles (○) indicate the positions of T_g, determined from the corresponding derivative curves. As $N_{A'}$ increases, the T_g remains the same (±1 °C). Compare Figure C.11 (LSO).

C-9 SCFT Calculations: LSO-N_C and LSL'-$N_{A'}$ Series

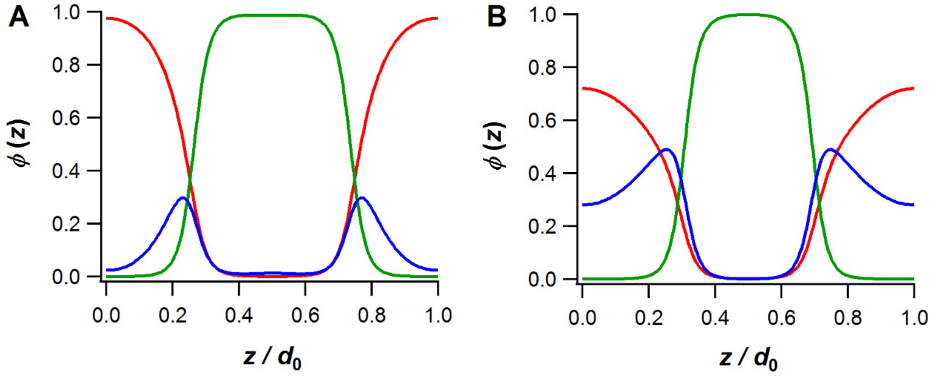

Figure C.13: SCFT composition profiles calculated over one lamellar period for two triblocks that self-assemble to LAM$_P$: (*A*) LSO-6 and (*B*) LSO-20. The relative segment concentrations $\phi(z)$ of each component are shown (red: PLA, green: PS, blue: PEO). SCFT predicts a small proportion of PEO blocks mixed in PS domains when N_C is small, consistent with the chain pullout model for the unusual d^* trend. Profiles were calculated using $\chi_{LS} = 0.080$, $\chi_{SO} = 0.049$, $\chi_{LO} = -0.010$, and different C block dispersities (Table C.4).

Table C.4: SCFT calculations for the lamellar period for LSO-N_C brush triblock terpolymers, in which N_A, N_B are fixed and N_C is varied. Calculations were performed using $\chi_{LS} = 0.080$, $\chi_{SO} = 0.049$, and $\chi_{LO} = -0.010$. The decrease in d^* can be attributed to the effects of molecular asymmetry and shielding of PLA-PS interactions by the PEO block, which are further enhanced by polydispersity of the PEO block.

Sample	**d^* Experiment[a] (nm)**	**d^* SCFT, monodisperse[b] (nm)**	**d^*, SCFT, polydisperse[c] (nm)**	**$Đ_C$[d]**
LSO-0	29.0	35.3	–[e]	–[e]
LSO-2	27.9	35.0	33.0	1.82
LSO-4	27.0	23.6	26.2	1.67
LSO-6	26.8	23.7	24.9	1.55
LSO-8	26.5	23.9	24.7	1.45
LSO-10	25.8	24.1	24.8	1.37
LSO-12	25.2	24.4	25.0	1.30
LSO-14	24.6	24.7	25.3	1.25
LSO-16	24.5	25.0	25.7	1.20
LSO-20	23.6	25.9	26.3	1.14

[a] Domain spacing, $d^* = 2\pi/q^*$, determined by SAXS and measured at 25 °C.

[b] Doman spacing predicted by SCFT when the polymers are assumed to be monodisperse ($Đ_C = 1.00$).

[c] Domain spacing predicted by SCFT when dispersity in the PEO block ($Đ_C > 1.00$) is introduced, according to the values of $Đ_C$ in the last column.

[d] Dispersity in the backbone length of the C block, calculated using $Đ_C = 1 + \exp(-N_C/10)$.

[e] Because LSO-0 does not have a C end block, polydisperse calculations were not performed.

Table C.5: SCFT calculations for the lamellar period for LSL'-$N_{A'}$ brush triblock terpolymers, in which N_A, N_B are fixed and $N_{A'}$ is varied. Calculations were performed using $\chi_{LS} = 0.080$. The decrease in d^* can be attributed to the effects of molecular asymmetry, which are further enhanced by polydispersity of the second PLA block.

Sample	d^* Experiment[a] (nm)	d^* SCFT, monodisperse[b] (nm)	d^*, SCFT, polydisperse[c] (nm)	$Đ_{A'}$[d]
LSL'-0	32.9	39.7	–[e]	–[e]
LSL'-2	31.3	38.4	35.3	1.82
LSL'-5	29.6	27.0	28.1	1.61
LSL'-7	28.6	27.3	28.1	1.50
LSL'-10	27.8	28.0	28.5	1.37
LSL'-12	27.4	28.5	28.9	1.30
LSL'-14	26.7	28.9	29.4	1.25
LSL'-17	26.6	29.6	30.0	1.18
LSL'-19	26.2	30.1	30.4	1.15
LSL'-24	25.7	31.3	31.7	1.09

[a] Domain spacing, $d^* = 2\pi/q^*$, determined by SAXS and measured at 25 °C.

[b] Doman spacing predicted by SCFT when the polymers are assumed to be monodisperse ($Đ_{A'} = 1.00$).

[c] Domain spacing predicted by SCFT when dispersity in the PEO block ($Đ_{A'} > 1.00$) is introduced, according to the values of $Đ_{A'}$ in the last column.

[d] Dispersity in the backbone length of the A' block, calculated using $Đ_{A'} = 1 + \exp(-N_{A'}/10)$.

[e] Because LSL'-0 does not have an A' end block, polydisperse calculations were not performed.

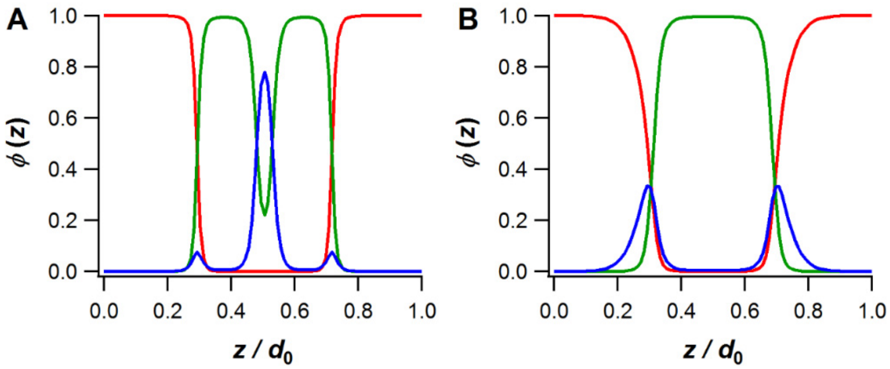

Figure C.14: SCFT composition profiles calculated over one lamellar period for a *linear* LSO triblock terpolymer in which each block has the same molecular weight as the corresponding block in LSO*. The relative segment concentrations $\phi(z)$ of each component are shown (red: PLA, green: PS, blue: PEO). Compare Figure 4.4: both brush and linear LSO triblock terpolymers show a transition from LAM$_3$ to LAM$_P$ controlled by the magnitude of χ_{LO}. Profiles were calculated using $\chi_{LS} = 0.080$, $\chi_{SO} = 0.049$, and $\chi_{LO} = 0.034 = \chi^C$ (the calculated transition between LAM$_3$ and LAM$_P$ where each phase is equally stable). (*A*) For large $\chi_{LO} > \chi^C$, SCFT predicts pure domains (LAM$_3$). (*B*) For small $\chi_{LO} < \chi^C$, SCFT predicts LAM$_P$.

C-10 Wide-Angle X-ray Scattering (WAXS)

Wide-angle X-ray scattering data was collected using a PANalytical X'Pert Pro. The wavelength of the X-ray beam was 1.54 Å. Samples were analyzed at 25 °C as neat powders, all prepared under the same conditions. Samples were scanned in the range $10° \leq 2\theta \leq 40°$, with step size 0.017°. Due to the geometry of the stage, minor peaks at 31.1° and 36.1° appear as artifacts.

LSO-N_C brush triblock terpolymers, their parent LS diblock (LSO-0), and PEO MM were characterized by WAXS (Figures 5.8, C.15). All samples were measured at room temperature as neat powders, prepared under the same conditions. WAXS data for LSO-4, LSO-14, and PEO MM were additionally collected (1) after heating to 60 °C at 1 °C/min and (2) after cooling to 30 °C at 10 °C/min. The percent crystallinity can be estimated based on such data collected in the molten, completely amorphous state (*i.e.*, above the melting temperature of PEO, T_m = 50 °C) and in the semicrystalline state.

Assuming an isotropic two-phase system comprising crystalline regions and amorphous regions, the scattered intensity I(s) (in sr^{-1}) consists of several contributions:

$$I(s) = \frac{1}{b_e^2}\frac{d\sigma}{d\Omega} = I_{cr}(s) + I_{am}(s) + I_{inc}(s) \quad \text{Eq. C-6}$$

where $s = (2/\lambda)\sin\theta$ is the magnitude of the scattering vector, $d\sigma/d\Omega$ is the differential scattering cross section, and b_e is the scattering length of an electron. The intensities $I_{cr}(s)$ and $I_{am}(s)$ contain information about the crystalline regions and amorphous regions of the sample, respectively, while the incoherent contribution $I_{inc}(s)$ contains no structural information. The ratio of $I_{cr}(s)$ to $I_{am}(s)$ reflects the weight fraction of crystallinity in a semicrystalline sample. In an approximation developed by Goppel and coworkers,[6] the intensity at a certain scattering vector s_0, chosen between Bragg reflections, is taken as part of $I_{am}(s)$. $I(s_0)$ is measured both in the semicrystalline sample (scry) and in a molten, completely amorphous sample (molt), and the crystallinity (x_{cr}) follows:

$$\frac{I_{scry}(s_0)}{I_{molt}(s_0)} \approx x_{am} = 1 - x_{cr} \quad \text{Eq. C-7}$$

The approach is accurate if the incoherent scattering and diffuse scattering can be neglected or subtracted. In our variable-temperature WAXS experiments, s_0 is chosen to correspond to the maximum in the amorphous halo ($2\theta = 20.2°$), between the reflections at $2\theta = 19.1°$ and 23.3° that correspond to the (120) and (032) reflections, respectively, from the monoclinic PEO lattice.[7] For LSO and PEO MM, $I_{\text{scry}}(s_0)$ was obtained from data collected at 30 °C, and $I_{\text{molt}}(s_0)$ was obtained from data at 60 °C.

LSO-4 and LSO-14 (two samples that self-assemble to LAM$_\text{P}$) comprise 6.8 wt% and 20.4 wt% PEO, respectively. From Eq. C-7, the crystalline weight fractions were estimated to be 3% and 6%, respectively. For the PEO MM, measured under the same conditions, the crystalline weight fraction is 50%. Crystallinity appears to be suppressed in the LSO brush triblock terpolymers. Various phenomena may contribute, such as (1) partial mixing of PLA and PEO, (2) the densely grafted bottlebrush architecture,[8] and (3) hard confinement of PEO between glassy PS microdomains.[9] Because the crystalline weight fraction is low throughout the series, we do not expect that crystallinity influences the domain spacing trend observed in LSO-N_C. Other work on PEO-containing block copolymers (Chapters 4 and 5) further supports this conclusion.

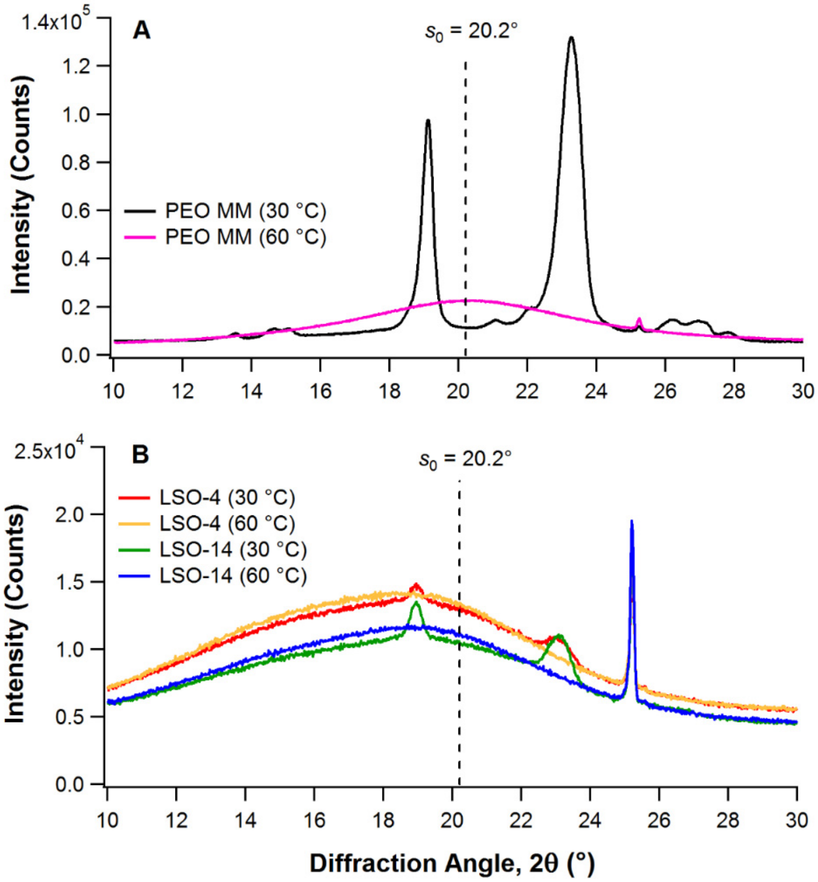

Figure C.15: Variable-temperature WAXS data for (*A*) PEO macromonomer (MM, M_n = 2000 g/mol) and (*B*) brush triblocks LSO-4 and LSO-14. For each sample, the intensity at scattering vector $s_0 = 2\theta = 20.2°$ was determined at 30 °C (before heating) and at 60 °C. At 60 °C, all samples are amorphous; the melting temperature of PEO is approximately 52 °C. The ratio of intensities at s_0 for crystalline and amorphous samples were used to estimate in the crystalline weight fractions (x_{cr}): x_{cr} in PEO MM is 50%, whereas x_{cr} in all LAM$_{\mathrm{P}}$-forming LSO samples is <10%.

References

(1) Sveinbjörnsson, B. R.; Weitekamp, R. A.; Miyake, G. M.; Xia, Y.; Atwater, H. A.; Grubbs, R. H. *Proc. Natl. Acad. Sci. U.S.A.* **2012**, *109*, 14332–14336.

(2) Dorgan, J. R.; Janzen, J.; Knauss, D. M.; Hait, S. B.; Limoges, B. R.; Hutchinson, M. H. *J. Polym. Sci., Part B: Polym. Phys.* **2005**, *43*, 3100–3111.

(3) Fetters, L. J.; Lohse, D. J.; Richter, D.; Witten, T. A.; Zirkel, A. *Macromolecules* **1994**, *27*, 4639–4647.

(4) Dalsin, S. J.; Rions-Maehren, T. G.; Beam, M. D.; Bates, F. S.; Hillmyer, M. A.; Matsen, M. W. *ACS Nano* **2015**, *9*, 12233–12245.

(5) Kim, J. U.; Matsen, M. W. *Macromolecules* **2009**, *42*, 3430–3432.

(6) Goppel, J. M.; Arlman, J. J. *Flow, Turbulence and Combustion* **1949**, *1*, 462–474.

(7) Takahashi, Y.; Tadokoro, H. *Macromolecules* **1973**, *6*, 672–675.

(8) Bates, C. M.; Chang, A. B.; Momčilović, N.; Jones, S. C.; Grubbs, R. H. *Macromolecules* **2015**, *48*, 4967–4973.

(9) Zhu, L.; Cheng, S. Z. D.; Calhoun, B. H.; Ge, Q.; Quirk, R. P.; Thomas, E. L.; Hsiao, B. S.; Yeh, F.; Lotz, B. *Polymer* **2001**, *42*, 5829–5839.